

PointConvFormer: Revenge of the Point-based Convolution

Wenxuan Wu^{1*}, Qi Shan², and Li Fuxin^{1,2}

¹ Oregon State University wuwen@oregonstate.edu

² Apple Inc. qshan,fl126@apple.com

Abstract. We introduce PointConvFormer, a novel building block for point cloud based deep neural network architectures. Inspired by generalization theory, PointConvFormer combines ideas from point convolution, where filter weights are only based on relative position, and Transformers which utilizes feature-based attention. In PointConvFormer, feature difference between points in the neighborhood serves as an indicator to re-weight the convolutional weights. Hence, we preserved the invariances from the point convolution operation whereas attention is used to select relevant points in the neighborhood for convolution. To validate the effectiveness of PointConvFormer, we experiment on both semantic segmentation and scene flow estimation tasks on point clouds with multiple datasets including ScanNet, SemanticKitti, FlyingThings3D and KITTI. Our results show that PointConvFormer substantially outperforms classic convolutions, regular transformers, and voxelized sparse convolution approaches with smaller, more computationally efficient networks. Visualizations show that PointConvFormer performs similarly to convolution on flat surfaces, whereas the neighborhood selection effect is stronger on object boundaries, showing that it got the best of both worlds.

1 Introduction

Depth sensors for indoor and outdoor 3D scanning have significantly improved in the last decade, in terms of both performance and affordability. Hence, their common output data format, 3D point cloud, has drawn significant attention from academia and industry in

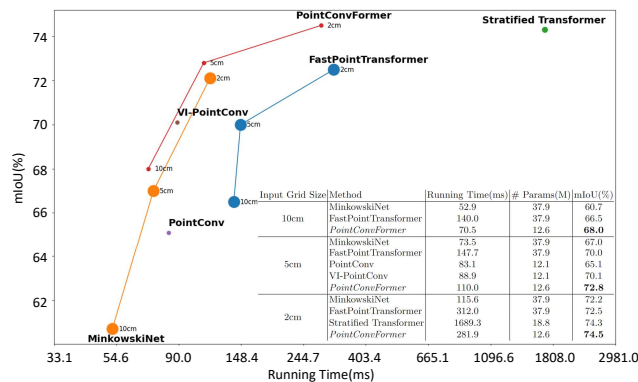


Fig. 1: **Performance vs. running time on ScanNet.** PointConvFormer achieves a state-of-the-art 74.5% mIoU while being efficient with way less learnable parameters. Larger dot indicates more learnable parameters. All results are reported on a single TITAN RTX GPU.

* Majority of the work done as an intern at Apple, Inc.

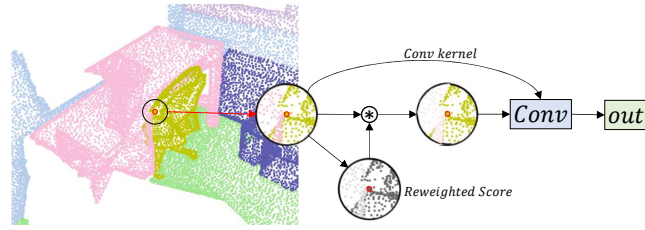


Fig. 2: **PointConvFormer** can be seen as a point convolution, but modulated by an attention weight for each point in the neighborhood, computed from the differences of current layer features between neighboring points

recent years. Understanding the 3D real world from point clouds can be applied to many application domains, such as robotics, autonomous driving, CAD, and AR/VR. However, unlike image pixels arranged in regular grids, 3D points are unstructured, which makes applying classic grid based Convolutional Neural Networks (CNNs) difficult.

Various approaches have been proposed in response to this challenge. [66,36,4,30,34] introduce interesting ways to project a 3D point cloud back to 2D image space to apply 2D convolution. These approaches relies heavily on the choice of projection planes, and have challenges in handling occlusions in the 3D space [93]. Another line of research directly voxelizes 3D space and apply 3D discrete convolution. These methods induce massive computation and memory overhead [46,63]. Sparse convolution operations [18,8] save a significant amount of computation by computing convolution only on occupied voxels.

Some approaches directly operate on point clouds without discretizing into grids [57,58,65,69,80,40]. [57,58] are pioneers which aggregate information on point clouds using max-pooling layers. Others proposed reordering the input points with a learned transformation [41], a flexible point kernel [69], and a convolutional operation that directly work on point clouds [75,80] by utilizing a multi-layer perceptron (MLP) to learn the convolution weights implicitly as a nonlinear transformation from the relative positions of the local neighbourhood.

The approach to directly work on points is appealing to us because it allows direct manipulation of the point coordinates, therefore being able to encode rotation/scale invariance/equivariance directly into the operation [91,40]. Besides, they should be more efficient models than voxel-based approaches, since in the latter approaches the need to keep e.g. $3 \times 3 \times 3$ convolution kernels leads to far sparser neighborhoods, and henceforth many more layers for the receptive fields to grow to the entire point cloud. Meanwhile, increasing the voxel size to reduce sparsity usually result in significantly worse recognition performance. However, so far the methods with the best efficiency-accuracy tradeoff have still been the sparse voxel-based approaches or a fusion between sparse voxel and point-based models.

We do not believe such a fusion would be necessary, since no matter the voxel-based or point-based representation, the information from the input is exactly the same. Besides, similar convolution operations can be performed in both the voxel and point-based representations. This leads us to question the component

that is indeed different between these representations: the construction of the local neighbourhood. Due to the irregular structure of point clouds, point-based representations [58,80] often utilizes the K-nearest neighbour(kNN) algorithm to compute the neighbourhood around each point. However, the shape of the kNN neighbourhood varies in different parts of the point cloud. Irrelevant points from other objects, noise and the background might be included in the neighbourhood, especially around object boundaries, which can be detrimental to the performance and the robustness of point-based models.

To improve the robustness of models with kNN neighborhoods, we refer back to generalization theory of CNNs, which indicated that points with significant feature correlation should be included in the same neighborhood [39]. A key idea in this paper is that feature correlation can be a way to filter out irrelevant neighbors in a kNN neighborhood while still performing convolution. We introduce PointConvFormer, which computes attention weights based on feature differences and use that to reweight the points in the neighborhood in a point-based convolutional model. PointConvFormer addresses the puzzle of how to define a “good” neighbourhood in point cloud processing for better representation and generalization.

Although the idea of using feature-based attention is not new, there are important differences between PointConvFormer and the recently popular vision transformers [14,93,54]. PointConvFormer combines features in the neighborhood with point-wise convolution, whereas Transformer attention models, usually adopts softmax attention in this step. However, softmax outputs a small amount of positive weights and a large amount of weights very close to zero, and is not able to generate negative coefficients in the aggregation step. In our formulation, because convolution is used for aggregation, both positive and negative weights are allowed. This is shown to be better than softmax attention in experiments. Another small insight we had was, when kNN neighborhood is used, the neighborhood itself is already small enough, hence we may no longer need the softmax mechanism to induce more extreme sparsity. In our experiments using the sigmoid activation on the attention weights for PointConvFormer have performed better than the softmax.

We evaluate PointConvFormer on two point cloud tasks, semantic segmentation and scene flow estimation. For semantic segmentation, experiment results on the indoor ScanNet [10] and the outdoor SemanticKitti [3] demonstrate superior performances over classic convolution and transformers with a more compact network. Such results show that, a model based on convolution with kNN neighborhoods can still achieve state-of-the-art performance if we use attention to filter out irrelevant points in the neighborhood. We also apply PointConvFormer as the backbone of PointPWC-Net [81] for scene flow estimation, and observe significant improvements on FlyingThings3D [47] and KITTI scene flow 2015 [52] datasets. We include ablation studies which explores the design space of PointConvFormer.

To summarize the main contributions:



Fig. 3: **Applications of PointConvFormer.** PointConvFormer can serve as the backbone for various 3D scene understanding tasks, such as semantic segmentation for indoor/outdoor scenes, and scene flow estimation from point clouds

- We introduce PointConvFormer which modifies convolution by an attention weight computed from the differences of local neighbourhood features. We further extend the PointConvFormer with a multi-head mechanism.
- We conduct thorough experiments on semantic segmentation tasks for both indoor and outdoor scenes, as well as scene flow estimation from 3D point clouds on multiple datasets. Results showed that PointConvFormer achieves state-of-the-art performance and is more efficient than other types of transformers and sparse voxel-based convolution. Extensive ablation studies are conducted to study the properties and design choices of PointConvFormer.

2 Related Work

We examine related work on voxel-based networks, point-based networks, and recent point transformer work for 3D scene understanding. We also review dynamic filtering for 2D images.

Voxel-based networks. Different from 2D images, 3D point clouds are unordered and scattered in 3D space. One of the trending approaches to process 3D point clouds is to voxelize the point clouds into regular 3D voxels. However, directly applying 3D convolution [46,63] onto the 3D voxels can incur massive computation and memory overhead, which limits its applications to large-scale real world scenarios. [60] propose to use unbalanced octrees with hierarchical partitions. The sparse convolution [18,8] reduces the convolutional overhead by only working on the non-empty voxels. However, this kind of approaches may suffer if the quantization of the voxel grid is too coarse. The best performances are achieved with high quantization resolutions (e.g. 2cm per voxel), which still have high memory consumption and lead to large models.

Point-based networks. There are plenty of work [57,58,80,40,65,76] focusing on directly processing point clouds without re-projection or voxelization. [57,58] propose to use MLPs followed by max-pooling layers to encode and aggregate point cloud features. However, max-pooling could lead to the loss of critical geometric information in the point cloud. A number of work [49,29,48,37,17,73] build a kNN graph from the point cloud and conduct message passing using graph convolution. Later on, [75,83,69,80,45,41,15,40] conduct continuous convolution on point clouds. [75] represents the convolutional weights with MLPs.

SpiderCNN [83] uses a family of polynomial functions to approximate the convolution kernels. [65] projects the whole point cloud into a high-dimensional grid for rasterized convolution. [80,69] formulate the convolutional weights to be a function of relative position in a local neighbourhood, where the weights can be constructed according to input point clouds. [40] improves over [80] by introducing hand-crafted viewpoint-invariant coordinate transforms on the relative position to increase the robustness of the network. Such an invariant approach is only possible with point-based networks where the convolutional weights are functions of the relative positions of points, and not possible with a voxel-based approach where one has no direct access to the coordinates as a generator of the filter weights.

Dynamic filters and Transformers. Recently, the design of dynamic convolutional filters [85,90,5,29,74,64,88,77,70,44,28,94] has drawn more attentions. This line of work [44,90,5,85] introduces different methods to predict convolutional filters, which are shared across the whole input. [29,88,77,70] propose to predict the complete convolutional filters for each pixel. However, their applications are constrained by their computational inefficiency and high memory usage. [94] introduces decoupled dynamic filters with respect to the input features on 2D classification and upsampling tasks. [64,67] propose to re-weight 2D convolutional kernels with a fixed Gaussian or Gaussian mixture model for pixel-adaptive convolution. Dynamic filtering share some similarities with the popular transformers, whose weights are functions of feature correlations. However, the dynamic filters are mainly designed for images instead of point clouds.

With recent success in natural language processing [13,11,71,79,87] and 2D images analysis [22,14,92,59], transformers have drawn more attention in the field of 3D scene understanding. Some work [35,43,86,82] utilize global attention on the whole point cloud. However, these approaches introduce heavy computation overhead and are unable to extend to large scale real world scenes, which usually contain over $100k$ points per point cloud scan. Recently, the work [93,54] introduce point transformer with local attention to reduce the computation overhead, which could be applied to large scenes. Compared to previous convolutional approaches, our PointConvFormer computes the weights with both the relative position and the feature difference. Compared to transformers, the attention of the PointConvFormer modulates convolution kernels and use the sigmoid activation instead of softmax. Experiments showed that our design significantly improves the performance of the networks.

3 PointConvFormer

3.1 Point Convolutions and Transformers

Given an input continuous signal $x(p) \in \mathbb{R}^{c_{in}}$ where $p \in \mathbb{R}^s$ with s being a small number (usually 2 for 2D images or 3 for 3D point clouds, but could be any arbitrary low-dimensional Euclidean space), $x(\cdot)$ can be sampled as a point cloud $P = \{p_1, \dots, p_n\}$ with the corresponding values $x_P = \{x(p_1), \dots, x(p_n)\}$,

where each $p_i \in \mathbb{R}^s$. The continuous convolution at point p is formulated as:

$$Conv(w, x)_p = \int_{\Delta p \in \mathbb{R}^s} \langle w(\Delta p), x(p + \Delta p) \rangle d\Delta p \quad (1)$$

where $w(\Delta p) \in \mathbb{R}^{c_{in}}$ is the continuous convolution weight function. Inspired by the continuous formulation of convolution, [62,80,76] discretize the continuous convolution on a neighbourhood of point p . Let $X_{p_i} \in \mathbb{R}^{c_{in}}$ be the input feature of p_i the discretized convolution on point clouds is written as:

$$X'_p = \sum_{p_i \in \mathcal{N}(p)} w(p_i - p)^\top X_{p_i} \quad (2)$$

where $\mathcal{N}(p)$ is a neighborhood that is normally chosen as the k -nearest neighbor or ϵ -ball neighborhood of the center point p . The function $w(p_i - p) : \mathbb{R}^s \mapsto \mathbb{R}^{c_{in}}$ can be approximated as an MLP and learned from data.

In PointConv [80], an efficient formulation was derived when $w(p_i - p)$ has a linear final layer $w(p_i - p) = W_l h(p_i - p)$, where $h(p_i - p) : \mathbb{R}^3 \mapsto \mathbb{R}^{c_{mid}}$ is the output of the penultimate layer of the MLP and $W_l \in \mathbb{R}^{c_{in} \times c_{mid}}$ is the learnable parameters in the final linear layer. We can equivalently change Eq. (2) on the neighbourhood $\mathcal{N}(p)$ into,

$$X'_p = \left\langle \text{vec}(W_l), \text{vec} \left\{ \sum_{p_i \in \mathcal{N}(p)} h(p_i - p) X_{p_i}^\top \right\} \right\rangle. \quad (3)$$

where $\text{vec}(\cdot)$ turns the matrix into a vector. Note that W_l represents parameters of a linear layer and hence independent of p_i . Thus, when there are c_{out} convolution kernels, n training examples with a neighborhood size of k each, there is no longer a need to store the original convolution weights $w(p_i - p)$ for each point in each neighborhood with a dimensionality of $c_{out} \times c_{in} \times k \times n$. Instead, the dimension of all the $h(p_i - p)$ vectors in this case is only $c_{mid} \times k \times n$, where c_{mid} is significantly smaller (usually 8 or 16) than $c_{out} \times c_{in}$ (could go higher than $10^2 \times 10^2$). This efficient PointConv enables applications to large-scale networks on 3D point cloud processing.

Recently, transformer architectures are popular with 2D images. 3D point cloud-based transformers have also been proposed (e.g. [93,54]). Transformers compute an attention model between points (or pixels) based on the features of both points and the positional encodings of them. Relative positional encoding was the most popular which encodes $w(p_i - p)$, similar to Eq. (2). It has been shown to outperform absolute positional encodings in many papers [61,9,93]. Adopting similar notations to Eq. (2), we can express the softmax attention model used in transformers as:

$$Attention(p) = \sum_{p_i \in \mathcal{N}(p)} \text{softmax}(\mathbf{q}(X_{p_i})\mathbf{k}(X_p) + w(p_i - p)) \cdot \mathbf{v}(X_{p_i}) \quad (4)$$

where $\mathbf{q}(\cdot)$, $\mathbf{k}(\cdot)$, $\mathbf{v}(\cdot)$ are transformation to the features to form the query, key and value matrices respectively, usually implemented with MLPs. One can see that

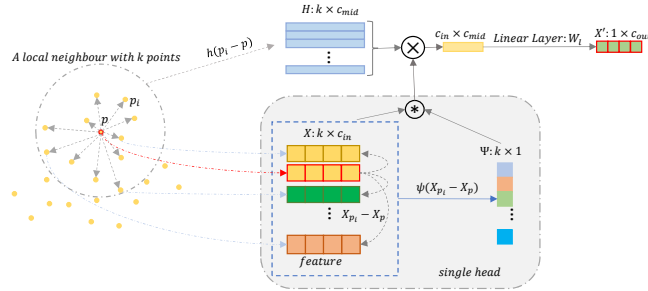


Fig. 4: **Details of the PointConvFormer Operation.** $h(p_i - p) : \mathbb{R}^3 \mapsto \mathbb{R}^{k \times c_{mid}}$ and $\psi(X_{p_i} - X_p) : \mathbb{R}^{c_{in} \times k} \mapsto \mathbb{R}^{k \times 1}$ are functions of the relative position $p_i - p$ and functions of differences of features. The weights of PointConvFormer combines the information from feature differences $X_{p_i} - X_p$ and relative position $p_i - p$.

there are similarities and differences between PointConv [80] and the attention model [71]. First, both employ $w(p_i - p)$, but in PointConv that is the sole source of the convolutional kernel which is translation-invariant. In attention models, the matching between the query transform $\mathbf{q}(X_{p_i})$ and the key transform $\mathbf{k}(X_p)$ of the features are also considered, which is no longer translation-invariant.

Another important difference to note is that in attention models the final attention value is an output from the softmax function. Note that softmax output has a range of $[0, 1]$ which is limited to **non-negative** weights at each point, which means the output of eq. (4) is a non-negative weighted average of the features of the input. To us, it is a bit curious why this is the right idea, as we tend to believe each neighborhood point could have positive and negative impacts to the features of the center point, and limiting it only to non-negative might be a dubious design choice.

We want to note that the $\mathbf{v}(\cdot)$ transform can be seen as a 1×1 convolution on the input features. It is common to insert 1×1 convolution layers between regular convolution layers in deep architectures (e.g. ResNet[20]), hence we could view it as an additional 1×1 convolution layer before the attention layer, hence we can compare the attention layer and PointConv without considering $\mathbf{v}(\cdot)$.

3.2 CNN Generalization Theory and The PointConvFormer Layer

We are interested to adopt the strengths of attention-based models, while exploring the design space where we still preserve some of the benefits of convolution and explore the possibility of having negative weights. To this end, we first look at theoretical insights in terms of which architecture would generalize well. We note the following bound proved in [39]:

$$\hat{G}_N(F) \leq C \max_{p' \in \mathcal{N}(p)} \sqrt{\mathbb{E}_{X,p}[(X_p - X_{p'})^2]} \quad (5)$$

where $\hat{G}_N(F)$ is the empirical Gaussian complexity on the function class F : a one-layer CNN followed by a fully-connected layer, and C is a constant. A

smaller Gaussian complexity leads to better generalization [1]. To minimize the Gaussian complexity bound in eq. (5), it can be seen that one should select points that has high feature correlation to belong to the same neighborhood. In images, nearby pixels usually have the highest color correlation [39], hence conventional CNNs achieve better generalization by choosing a small local neighborhood (e.g. 3×3). In 3D point clouds, as mentioned in the introduction, our problem is that noisy points can be included in the kNN neighborhood, which reduces feature correlation and henceforth worsens the generalization bound. This motivates us to attempt to filter out those noisy points by explicitly checking their $X_p - X_{p'}$, hence keeping only the relevant points in the CNN neighborhood and improve generalization.

Inspired by the discussion above, We define a convolution operation with its weights as functions of both the relative position $p_i - p$ and the feature difference $X_{p_i} - X_p$. Hence, PointConvFormer layer of a point p with its neighbourhood $\mathcal{N}(p)$ can be written as:

$$X'_p = \sum_{p_i \in \mathcal{N}(p)} w(p_i - p)^\top \psi(X_{p_i} - X_p) X_{p_i} \quad (6)$$

where the function $w(p_i - p)$ is the same as defined in Eq. (2), the function $\psi(X_{p_i} - X_p) : \mathbb{R}^{c_{in}} \mapsto \mathbb{R}$ is the function of feature differences $X_{p_i} - X_p$, which projects the differences of features in a local neighbourhood to a re-weighted attention $\psi(X_{p_i} - X_p) \in \mathbb{R}$, similar to the attention scores in point transformers [93].

If we fix the function $\psi(X_{p_i} - X_p) = 1$, the PointConvFormer layer is equivalent to Eq. (3), which reduces to traditional convolution. In eq.(6) $\psi(X_{p_i} - X_p)$ is approximated with another MLP followed by a activation layer, such as softmax, sigmoid, or ReLU. We explore the optimal choice of the MLP structure in our ablation studies. As a result, the function $w(p_i - p)$ learns the weights respect to the relative positions, and the function $\psi(X_{p_i} - X_p)$ learns the differences between the features of point p and its neighbourhood, which works similarly to the attention in transformer. However, different from the transformer whose non-negative weights are directly used as a weighted average on the input, the output of $\psi(X_{p_i} - X_p)$ modifies the convolutional filter $w(p_i - p)$, which allows each neighborhood point to have both positive and negative contributions.

Although we choose the above formulation based on generalization theory, we can also directly adopt the dot-product attention in ψ , which would lead to:

$$X'_p = \sum_{p_i \in \mathcal{N}(p)} w(p_i - p)^\top \psi(\mathbf{q}(X_{p_i})\mathbf{k}(X_p)) X_{p_i} \quad (7)$$

. The advantage of the dot-product attention is that the inner product between \mathbf{q} and \mathbf{k} is one-dimensional, hence only an activation is needed for the pairwise operations, whereas the formulation in eq.(6) inputs a multi-channel input to ψ . Hence, the computational cost and memory usage of eq. (7) are slightly smaller. Note that the convolution part $w(p_i - p)$ still exists hence this is still different from regular attention eq. (4). In our ablation studies, we find that the feature

difference version as in (6) achieves slightly better performance than this one. Hence, users can choose between these two formulations based on practical needs.

Since $\psi(X_{p_i}, X_p)$ is a re-weighted score that works on the input feature, we adopt the same approach in PointConv [80] to create an efficient version of the PointConvFormer layer. Following eq.(3), we have:

$$X'_p = W_l \sum_{p_i \in \mathcal{N}(p)} h(p_i - p) \psi(X_{p_i}, X_p) X_{p_i}^\top \quad (8)$$

where W_l and $h(\cdot)$ are the same as in Eq. (3) and either of the formulation eq.(6) or eq.(7) can be used. The PointConvFormer structure is illustrated in Fig. 4.

3.3 Multi-Head Mechanism

As in Eq.(8), the weight function $\psi(X_{p_i} - X_p) : \mathbb{R}^{c_{in}} \mapsto \mathbb{R}$ learns the relationship between the center point feature $X_p \in \mathbb{R}^{c_{in}}$ and its neighbourhood features $X_{p_i} \in \mathbb{R}^{c_{in}}$, where c_{in} is the number of the input feature dimension. To increase the representation power of the PointConvFormer, we attempt to use the multi-head mechanism to learn different types of neighborhood filter mechanisms, in order to improve the representation capabilities. As a result, the function $\psi : \mathbb{R}^{c_{in}} \mapsto \mathbb{R}$ becomes a set of functions $\psi_i : \mathbb{R}^{c_{in}} \mapsto \mathbb{R}$ with the number of heads being h , and $i \in \{1, \dots, h\}$.

4 Semantic Segmentation

To demonstrate the effectiveness of the proposed PointConvFormer in real world point clouds, we adopt the PointConvFormer to large-scale semantic segmentation tasks. In this section, we introduce the network structure and the main network components used for the segmentation.

4.1 PointConvFormer Block

To build deep neural network for various computer vision tasks, we construct bottleneck residual blocks with PointConvFormer layer as its main components. The detailed structures of the residual blocks are illustrated in Fig. 5. The input of the residual block is the input point features $X \in \mathbb{R}^{c_{in}}$ along with its coordinates $p \in \mathbb{R}^3$. The residual block uses a bottleneck structure, which consists of two branches. The residual branch is a linear layer, followed by PointConvFormer layer, followed by another linear layer. Following ResNet [20,69], we use one-fourth of the input channels in the first linear layer, conduct PointConvFormer with the smaller number of channels, and finally upsample to the amount of output channels. This is different from transformers which usually utilizes an expansion-squeeze strategy similar to MobileNet [21]. We have found our ResNet-style strategy to reduce the computational cost while maintaining high accuracy. The shortcut branch can be formulated in three different ways

depending on the output feature size. If the output feature has the same cardinality and dimensionality, the shortcut branch is just a identity mapping. If the output feature has the same cardinality but with different dimensionality, the shortcut branch is a linear mapping. If the output feature has different cardinality, e.g. when the point cloud is downsampled, the shortcut branch can use max-pooling layers to aggregate features.

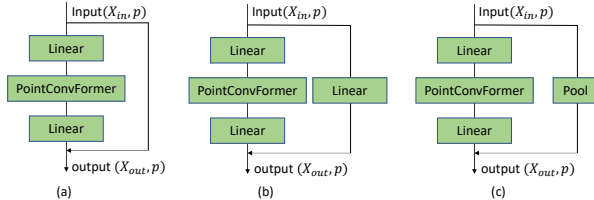


Fig. 5: **The residual blocks of PointConvFormer.** We use Linear layers and pooling layers to change the dimensionality and cardinality of the shortcut to match the output of the residual branch.

4.2 Backbone Structure

In this work, we adopted a general U-Net structure with residual blocks in the encoding layers as our backbone model, where the point clouds are gradually downsampled to coarse resolution, then gradually upsampled to its original resolution with the help of finer level features. Please refer to the supplementary for detailed network structure. We use the grid-subsampling method [69] to down-sample the point clouds as in [69] along with the PointConvFormer blocks to encode features. For upsampling layers, we are unable to apply PointConvFormer because for points that do not exist in the downsampled cloud, their features are not present. To address this issue, we note that in eq. (3) of PointConv, p itself does not have to belong to $\mathcal{N}(p)$, thus we can just apply PointConv layers for deconvolution without features X_p as long as coordinates p are known.

5 Scene Flow estimation from Point Clouds

In this section, we adopt our PointConvFormer to scene flow estimation from 3D point clouds. Scene flow is the 3D displacement vector between each surface in two consecutive frames. As a fundamental tool for low-level understanding of the world, scene flow can be used in many 3D applications, such as autonomous driving, virtual reality, etc. Traditionally, scene flow was estimated directly from RGB/RGBD data [27,50,72]. However, with the recent development of 3D sensors such as LiDAR and 3D deep learning techniques, there is increasing interest on directly estimating scene flow from 3D point clouds [42,19,81,56,78]. In this work, we are interested in adopting the PointConvFormer into the PointPWC-Net [81], which utilizes a coarse-to-fine framework for scene flow estimation.

PointPWC-Net [81] is a coarse-to-fine network design, which aims to iteratively refine the scene flow estimation. It mainly contains 5 modules, including the feature pyramid network, cost volume layers, upsampling layers, warping layers, and the scene flow predictors. The feature pyramid network is built with multiple PointConv [80] layers to encode point features in different resolutions. The cost volume layers compute the learned cost volume in the 3D space. The upsampling layers and warping layers interpolate the coarse scene flow to a finer level and warp the target point cloud, respectively. Finally, the scene flow predictors estimate scene flow for each resolution. To adopt our PointConvFormer to the PointPWC-Net, we replace the PointConv in the Feature pyramid layers with the PointConvFormer and keep the rest of the structure the same as the original version of PointPWC-Net for fair comparison.

6 Experiments

In this section, we conduct experiments in a number of domains and tasks to demonstrate the effectiveness of the proposed PointConvFormer. For 3D semantic Segmentation, we use the challenging ScanNet [10], a large-scale indoor scene dataset, and the SemanticKitti dataset [3], a large-scale outdoor scene dataset. Besides, we conduct experiments on the scene flow estimation from 3D point clouds with the synthetic FlyingThings3D dataset [47] for training and KITTI scene flow 2015 dataset [52] for testing. We also conduct ablation studies to explore the properties of the PointConvFormer.

Implementation Details. We implement PointConvFormer in PyTorch [55]. As in [40], the viewpoint-invariant coordinate transform in [40] is concatenated with the relative coordinates as the input to the $w(\cdot)$ function. We use the Adam optimizer with (0.9, 0.999) betas and 0.0001 weight decay. For the ScanNet dataset, we train the model with an initial learning rate 0.001 and dropped to 0.5x for every 80 epochs for 400 epochs. For the SemanticKitti dataset, the model is trained with an initial learning rate 0.001 and dropped to 0.5x for every 8 epochs for 40 epochs. Both semantic segmentation tasks are trained with weighted cross entropy loss. To ensure fair comparison with published approaches, we did not employ the recent Mix3D augmentations [53] which would improve performance for all methods. For the scene flow estimation, we follow the exact same training pipeline in [81] for fair comparison.

6.1 Indoor Scene Semantic Segmentation

We conduct 3D semantic scene segmentation on the ScanNet [10] dataset. We use the official split with 1,201 scenes for training and 312 for validation. MinkowskiNet42 [8], SparseConvNet [18] are compared as representative voxel-based methods. The PointNet [57], PointConv [80], VI-PointConv [40], PointASNL [84], and KPConv [69] are chosen as representative point-based methods. Recently, there are work adopting transformer to point clouds. We chose the Point Transformer [93] and the fast point transformer [54] as representative transformer

based methods. Since the Point Transformer does not report their results on the ScanNet dataset, we adopt their point transformer layer (a standard multi-head attention layer) with the same network structure as ours. Hence, it serves as a direct comparison between PointConvFormer and multi-head attention. There exists some other approaches [7,25,26,32] which use additional inputs, such as 2D images, which benefit from ImageNet [12] pre-training that we do not use. Hence, we excluded these methods from comparison, accordingly.

Following [54], we conduct experiments on different input voxel sizes, reported in Table 1. Since we use grid-subsampling [69] with different grid sizes to downsample the input point cloud, voxel size is also a parameter in our network. Although, we still utilize kNN neighborhoods which always have k neighbors whereas sparse convolution could have far fewer points in their neighborhood, hence needing more layers than us to get the same receptive field. According to Table. 1, our PointConvFormer achieves best results with different input grid size. Especially, our PointConvFormer outperforms MinkowskiNet42 [8] by a very significant 7.6% with 10cm input grid, 6.2% with 5cm input grid, and 2.3% with 2cm input grid. Comparing with Point Transformer [93] and PointConv [80]/VI-PointConv [40], our PointConvFormer achieves significant improvement with the same network backbone.

Table 1: **Comparison with different input voxel size.** We compare the results on the ScanNet [10] validation set with different input voxel size. [†] means the results are reported in [54]. We use grid subsampling [69] to downsample the input point clouds, which is similar to voxelization. However, we still use kNN neighborhood after downsampling which is different from the voxel neighborhood used in other approaches. * means we implemented it on the same network structure as PointConvFormer, hence it also serves as an ablation comparing regular self-attention layers and convolutional layers with PointConvFormer layers

Methods	Voxel/grid size	# Params(M)	Input	mIoU(%)
MinkowskiNet42 [†] [8]	10cm	37.9	Voxel	60.4
Fast Point Transformer [54]	10cm	37.9	Voxel	65.3
PointConvFormer(ours)	10cm	12.6	Point	68.0
MinkowskiNet42 [†] [8]	5cm	37.9	Voxel	66.6
Fast Point Transformer [54]	5cm	37.9	Voxel	70.1
Point Transformer*	5cm	10.7	Point	68.0
PointConv*	5cm	12.1	Point	65.1
VI-PointConv*	5cm	12.1	Point	70.1
PointConvFormer(ours)	5cm	12.6	Point	72.8
MinkowskiNet42 [†] [8]	2cm	37.9	Voxel	72.2
Fast Point Transformer [54]	2cm	37.9	Voxel	72.0
PointConvFormer(ours)	2cm	12.6	Point	74.5

Besides, we further evaluate our PointConvFormer with other state-of-the-art methods, shown in Table 2. From the results shown in Table 2, we can see

that our proposed PointConvFormer achieves the best performance among the point-based methods, outperforming the best point convolution based method KPConv [69] by 3.6% in mIoU. Besides, our PointConvFormer achieves slightly better results than the sparse voxel-based methods, including the MinkowskiNet42, with only 40% of the number of learnable parameters of MinkowskiNet42. In the result visualizations shown in Fig. 6, we observe that PointConvFormer is able to achieve better predictions with fine details comparing with PointConv [80] and Point Transformer [93]. Interestingly, it seems that PointConvFormer is usually able to find the better prediction out of PointConv [80] and Point Transformer [93], showing that its novel design brings the best out of both operations.

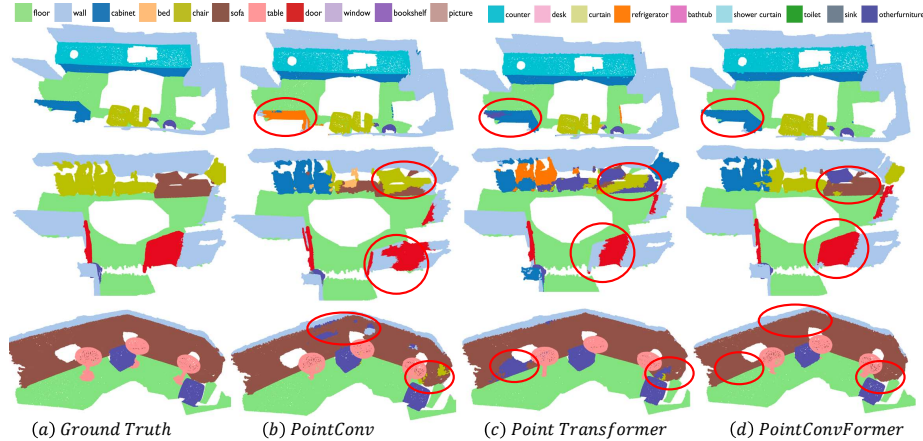


Fig. 6: **ScanNet result visualization.** We visualize the ScanNet prediction results from our PointConvFormer, PointConv [80] and Point Transformer [93]. The **red** ellipses indicates the improvements of our PointConvFormer over other approaches. Points with ignore labels are filtered for a better visualization. (Best viewed in color)

6.2 Outdoor Scene Semantic Segmentation

The SemanticKitti [3,16] dataset is a large-scale street view point cloud dataset built upon the KITTI Vision Odometry Benchmark [16]. The dataset is collected in Germany with Velodyne-HDLE64 LiDAR, and consists of 43,552 point cloud scans sampled from 22 sequences in driving scenes. Each point cloud scan contains 10 – 13k points. We follow the training and validation split in [3] and 19 classes are used for training and evaluation. The training set includes 19,130 scans, and there are 4,071 scans in sequence 08) for validation. For each 3D point, only the (x, y, z) coordinates are given without any color information. It is a challenging dataset because the scanning density is uneven as faraway points are more sparse in LIDAR scans.

Table 3 reports the results on the semanticKitti dataset. Because this work mainly focus on the basic building block, PointConvFormer, which is applicable

Table 2: **Semantic segmentation results on ScanNet dataset.** We compare both the ScanNet [10] validation set and test set. The numbers for test set are from the official ScanNet benchmark.

Methods	# Params(M)	Input	Runtime(ms)	Val mIoU(%)	Test mIoU(%)
PointNet++ [58]	-	Point	-	53.5	55.7
PointCNN [41]	-	point	-	-	45.8
PointConv [80]	-	Point	83.1	65.1	66.6
KPConv <i>deform</i> [69]	14.9	Point	-	69.2	68.4
PointASNL [84]	-	Point	-	63.5	66.6
RandLA-Net [23]	-	point	-	-	64.5
VI-PointConv [40]	15.5	Point	88.9	70.1	67.6
SparseConvNet [18]	-	Voxel	-	69.3	72.5
MinkowskiNet42 [8]	37.9	Voxel	115.6	72.2	73.6
PointTransformer [93,33]	-	point	-	70.6	-
Fast Point Transformer [54]	37.9	Voxel	312.0	72.0	-
Stratified Transformer [33]	18.8	point	1689.3	74.3	74.7
PointConvFormer(ours)	12.6	Point	281.9	74.5	74.9

to any kind of 3D point cloud data, of deep neural network, we do not compare with work [95,6] whose main novelties work mostly on LiDAR datasets due to the additional assumption that there are no occlusions from the bird-eye view. We use a simple U-Net structure for semantic segmentation as described in Sec. 4.2 which has less parameters than most other high-performing networks. From the table, one can see that our PointConvFormer outperforms both point-based methods and point+voxel fusion methods. Especially, our method obtains better results comparing with SPVNAS [68], which utilizes the network architecture search (NAS) techniques and fuses both point and voxel branches. We did not utilize any NAS in our system which would only further improve our performance.

Table 3: **Semantic segmentation results on SemanticKitti validation set.**

Method	#MACs(G)	# Param.(M)	Input	mIoU(%)
RandLA-Net [24]	66.5	1.2	Point	57.1
FusionNet [89]	-	-	Point+Voxel	63.7
KPRNet [31]	-	-	Point+Range	64.1
MinkowskiNet [8]	113.9	21.7	Voxel	61.1
SPVCNN [68]	118.6	21.8	Point+Voxel	63.8
SPVNAS [68]	64.5	10.8/12.5	Point+Voxel	64.7
PointConvFormer(ours)	91.1	8.1	Point	67.1

6.3 Scene Flow Estimation from Point Clouds

Besides the semantic segmentation tasks, we also conduct experiments on scene flow estimation directly from 3D point clouds using the PointPWC-Net with PointConvFormer, as introduced in Sec. 5. For simplicity, we name the new network ‘PCFPWC-Net’ where PCF stands for PointConvFormer. To train the PCFPWC-Net, we use the multi-scale supervised loss [81] and follow the training pipeline in [81]. For a fair comparison, we use the same dataset configurations as in [81]. The model is first trained on FlyingThings3D [48], which is a large synthetic image dataset for scene flow estimation. The 3D point clouds are reconstructed from image pairs with the depth map provided in the dataset following [19]. As a result, the training dataset contains 19,640 pairs of point clouds, and the evaluation dataset contains 3,824 pairs of point clouds. We adopt the same hyper-parameters used in [81]. There are 4 pyramid levels in PCFPWC-Net. The model is trained with a starting learning rate of 0.001 and dropped by half every 80 epochs. After training on FlyingThings3D, we directly evaluate the trained model on the real world KITTI Scene Flow dataset [51,52] to test the generalization capabilities of our model. We follow the same preprocessing step in [19] and obtain 142 valid scenes for evaluation. For comparison, we use the same metrics as [81], which uses $EPE3D(m)$ as the main metric, $Acc3DS$, $Acc3DR$, $Outliers3D$, $EPE2D(px)$, $Acc2D$ for further comparison. Please check supplementary for details on the definition of those metrics.

Table 4: **Evaluation results on FlyingThings3D and KITTI dataset.** All approaches are trained on FlyingThings3D with the supervised loss. On KITTI, the models are directly evaluated on KITTI without any fine-tuning.

Dataset	Method	$EPE3D(m)\downarrow$	$Acc3DS\uparrow$	$Acc3DR\uparrow$	$Outliers3D\downarrow$	$EPE2D(px)\downarrow$	$Acc2D\uparrow$
Flyingthings3D	FlowNet3D [42]	0.1136	0.4125	0.7706	0.6016	5.9740	0.5692
	SPLATFlowNet [65]	0.1205	0.4197	0.7180	0.6187	6.9759	0.5512
	HPLFlowNet [19]	0.0804	0.6144	0.8555	0.4287	4.6723	0.6764
	HCRF-Flow [38]	0.0488	0.8337	0.9507	0.2614	2.5652	0.8704
	FLOT [56]	0.052	0.732	0.927	0.357	-	-
	PV-RAFT [78]	0.0461	0.8169	0.9574	0.2924	-	-
	PointPWC-Net [81]	0.0588	0.7379	0.9276	0.3424	3.2390	0.7994
	PCFPWC-Net(ours)	0.0416	0.8645	0.9658	0.2263	2.2967	0.8871
KITTI	FlowNet3D [42]	0.1767	0.3738	0.6677	0.5271	7.2141	0.5093
	SPLATFlowNet [65]	0.1988	0.2174	0.5391	0.6575	8.2306	0.4189
	HPLFlowNet [19]	0.1169	0.4783	0.7776	0.4103	4.8055	0.5938
	HCRF-Flow [38]	0.0531	0.8631	0.9444	0.1797	2.0700	0.8656
	FLOT [56]	0.056	0.755	0.908	0.242	-	-
	PV-RAFT [78]	0.0560	0.8226	0.9372	0.2163	-	-
	PointPWC-Net [81]	0.0694	0.7281	0.8884	0.2648	3.0062	0.7673
	PCFPWC-Net(ours)	0.0479	0.8659	0.9332	0.1731	1.7943	0.8924

From Table 4, we can see that our proposed PCFPWC-Net outperforms previous methods in almost all the evaluation metrics. Comparing with PointPWC-Net [81], our PCFPWC-Net achieves around 10% improvement in $EPE3D$ and $EPE2D$ on the FlyingThings3D, around 10% in $Acc3DS$ and $Acc2D$. On the

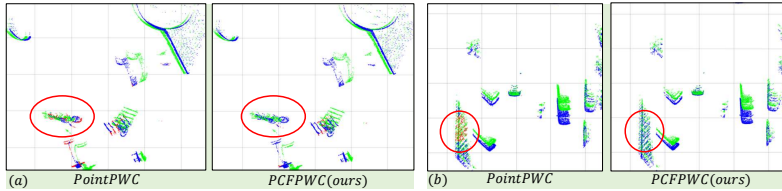


Fig. 7: **Qualitative comparison between PointPWC-Net and PCFPWC-Net.** (a) is the visualization of the FlyingThings3D dataset. (b) is the visualization of the KITTI dataset. Green points are the source point cloud. Blue points are the points warped by the correctly predicted scene flow. The predicted scene flow belonging to Acc3DR is regarded as a correct prediction. For the points with incorrect predictions, we use the ground truth scene flow to warp them and the warped results are shown as red points. (Best viewed in color.)

KITTI dataset, our PCFPWC-Net also shows strong result for scene flow estimation by improving the EPE3D by more than 30% (0.0694 \mapsto 0.0479) over PointPWC-Net [81]). Fig. 7 illustrates the qualitative results of PCFPWC-Net for both FlyingThings3D and KITTI dataset.

6.4 Ablation Studies

In this section, we perform thorough ablation experiments to investigate our proposed PointConvFormer. The ablation studies are conducted on the ScanNet [10] dataset. For efficiency, we downsample the input point clouds with a grid-subsampling method [69] with a grid size of 10cm as in [54].

Number of neighbours. We first conduct experiments on the neighbourhood size k in the PointConvFormer for feature aggregation. The results are reported in Table. 5. The best result is achieved with a neighbourhood size of 16. However, larger neighbourhood size of 32, 64 gives worse result, which may be caused by introducing excessive less relevant features in the neighbourhood [93].

Table 5: **Ablation Study.** Number of neighbours in each local neighbourhood.

Neighbourhood Size	4	8	16	32	64
mIoU(%)	63.00	68.10	69.16	68.54	67.41

Table 6: **Ablation Study.** Number of heads.

Number of Head	1	2	4	8	16
mIoU(%)	68.32	68.77	68.84	69.16	68.72

Number of heads in ψ . As described in Sec. 3.3, our PointConvFormer could employ the multi-head mechanism to further improve the representation capabilities of the model. We conduct ablation experiments on the number of heads in the PointConvFormer. The results are shown in Table. 6. From Table. 6, we find that PointConvFormer achieves the best result with 8 heads.

The structure of MLP in ψ . We conduct experiments to figure out the optimal design of the MLP for the function ψ in PointConvFormer. The ablations contain two parts: the number of layers in MLP and the last regularization function of MLP. Most of the attention based methods use *softmax* to normalize the attention score. In this experiments, we also test *sigmoid* and *ReLU*. Table. 7 and Table. 8 report the ablation results. From Table. 7, we find that our

PointConvFormer achieves reasonable results even with one hidden layer in the MLP of ψ , with the best results obtained with two hidden layers in the MLP. In Table. 8, the *sigmoid* activation function obtains the best performance. Interestingly, the performance becomes worse with *softmax*. This might be because that in the softmax function, attention scores have to be nonnegative and sum to 1, which usually results in too much sparsity and is not suitable in combination with a kNN neighborhood.

Different attention method. As described in Sec. 3.2, our PointConvFormer is a combination of convolution and transformer. There are mainly two version of attention: eq.(6) and eq.(7). In most of the paper we adopt the subtractive attention as in (6). We show the results comparing these formulations in Table. 9. The experiment results show that the feature difference achieves better results, which are also confirmed in [93]. Note that switching the softmax activation to sigmoid also helps the QKV version significantly. The QKV version has a bit more parameters due to the two MLPs for Q and K instead of a single one as in eq.(6). It in principle uses a bit less memory and computation during inference, but the savings is not very significant due to the small neighborhood size of $K = 16$.

Table 7: **Ablation Study.** Number of layers in MLP of ψ .

Number of layers	1	2	3	4
mIoU(%)	68.53	69.16	68.23	68.16

Table 8: **Ablation Study.** Regularization function.

Regularization	Softmax	ReLU	Sigmoid
mIoU(%)	68.57	68.48	69.16

Table 9: **Ablation Study.** Dot-product attention vs. additive attention.

Method (<i>same backbone</i>)	#Params(M)	#MACs(G)	mIoU(%)
PointConvFormer(QKV, softmax activation)	13.1	4.7	67.21
PointConvFormer(QKV, sigmoid activation)	13.1	4.7	68.73
PointConvFormer(subtractive attention)	12.6	4.7	69.16

6.5 Visualization of Reweighted Scores

In order to actually see what the reweighted score learn from the dataset, we visualize the difference of the learned reweighted score for some example scenes in the ScanNet [10] dataset. The difference is computed by $score_{max} - score_{min}$, where $score_{max}$ is the maximal $\psi(\cdot)$ in the neighbourhood and $score_{min}$ is the minimum. A larger difference indicates significant neighborhood filtering efforts. Otherwise, a smaller difference indicates $\psi = constant$ in the local neighbourhood. With constant or nearly constant reweighted scores throughout the neighbourhood, the PointConvFormer would reduce to regular point convolution. We

visualize the difference in Fig. 8 and Fig. 9 with *hot* colormap. From Fig. 8 and Fig. 9, we can see that higher differences happen mostly in object boundaries. For smooth surfaces and points from the same class, the difference of reweighted scores is low. This visualization further confirms that PointConvFormer is able to utilize feature differences to conduct neighborhood filtering according to the specifics of each neighborhood.

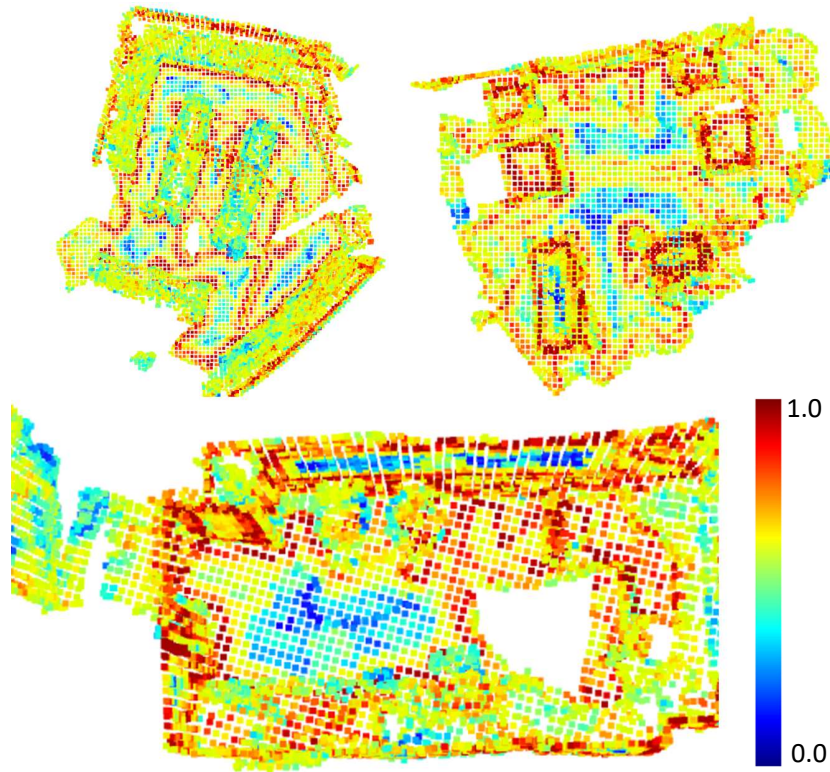


Fig. 8: **Visualization of reweighted scores(part 1)**. We visualize the difference of the learned reweighted scores in each neighbourhood. The difference is compute by $score_{max} - score_{min}$, where $score_{max}$ is the maximum reweighted score in the neighbourhood and $score_{min}$ is the minimum. More blue means the final operation is more similar to regular point convolution and more red means the neighborhood is more strongly filtered. (Best viewed in color.)

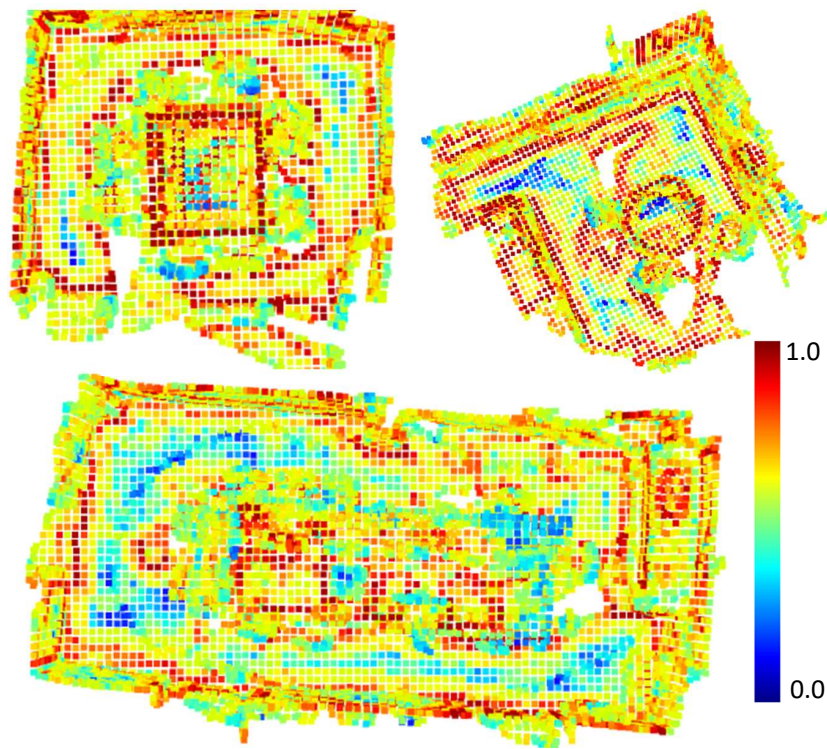


Fig. 9: **Visualization of reweighted scores(part 2)**. We visualize the difference of the learned reweighted scores in each neighbourhood. The difference is compute by $score_{max} - score_{min}$, where $score_{max}$ is the maximum reweighted score in the neighbourhood and $score_{min}$ is the minimum. More blue means the final operation is more similar to regular point convolution and more red means the neighborhood is more strongly filtered. (Best viewed in color.)

7 Conclusion

In this work, we propose a novel point cloud layer, PointConvFormer, which can be widely used in various computer vision tasks. Unlike traditional convolution of which convolutional kernels are functions of the relative position, the convolutional weights of the PointConvFormer are modified by feature differences. By taking the feature differences into account, the PointConvFormer incorporates benefits of attention models, which could help the network to focus on points with high feature correlation during feature encoding. Thorough experiments on a number of point cloud tasks showed that PointConvFormer significantly outperforms traditional point-based operations and outperforms other voxel-based or point-voxel fusion approaches, with significantly less trainable parameters than other voxel-based or fusion approaches.

References

1. Bartlett, P.L., Mendelson, S.: Rademacher and gaussian complexities: Risk bounds and structural results. *Journal of Machine Learning Research* **3**(Nov), 463–482 (2002)
2. Behley, J., Garbade, M., Milioto, A., Quenzel, J., Behnke, S., Stachniss, C., Gall, J.: SemanticKITTI: A Dataset for Semantic Scene Understanding of LiDAR Sequences. In: *Proc. of the IEEE/CVF International Conf. on Computer Vision (ICCV)* (2019)
3. Behley, J., Garbade, M., Milioto, A., Quenzel, J., Behnke, S., Stachniss, C., Gall, J.: Semantickitti: A dataset for semantic scene understanding of lidar sequences. In: *Proceedings of the IEEE/CVF International Conference on Computer Vision*. pp. 9297–9307 (2019)
4. Chen, X., Ma, H., Wan, J., Li, B., Xia, T.: Multi-view 3d object detection network for autonomous driving. In: *Proceedings of the IEEE conference on Computer Vision and Pattern Recognition*. pp. 1907–1915 (2017)
5. Chen, Y., Dai, X., Liu, M., Chen, D., Yuan, L., Liu, Z.: Dynamic convolution: Attention over convolution kernels. In: *Proceedings of the IEEE/CVF Conference on Computer Vision and Pattern Recognition*. pp. 11030–11039 (2020)
6. Cheng, R., Razani, R., Taghavi, E., Li, E., Liu, B.: 2-s3net: Attentive feature fusion with adaptive feature selection for sparse semantic segmentation network. In: *Proceedings of the IEEE/CVF conference on computer vision and pattern recognition*. pp. 12547–12556 (2021)
7. Chiang, H.Y., Lin, Y.L., Liu, Y.C., Hsu, W.H.: A unified point-based framework for 3d segmentation. In: *2019 International Conference on 3D Vision (3DV)*. pp. 155–163. IEEE (2019)
8. Choy, C., Gwak, J., Savarese, S.: 4d spatio-temporal convnets: Minkowski convolutional neural networks. In: *Proceedings of the IEEE Conference on Computer Vision and Pattern Recognition*. pp. 3075–3084 (2019)
9. Chu, X., Tian, Z., Zhang, B., Wang, X., Wei, X., Xia, H., Shen, C.: Conditional positional encodings for vision transformers. *arXiv preprint arXiv:2102.10882* (2021)
10. Dai, A., Chang, A.X., Savva, M., Halber, M., Funkhouser, T., Nießner, M.: Scannet: Richly-annotated 3d reconstructions of indoor scenes. In: *Proc. Computer Vision and Pattern Recognition (CVPR), IEEE* (2017)
11. Dai, Z., Yang, Z., Yang, Y., Carbonell, J., Le, Q.V., Salakhutdinov, R.: Transformer-xl: Attentive language models beyond a fixed-length context. *arXiv preprint arXiv:1901.02860* (2019)
12. Deng, J., Dong, W., Socher, R., Li, L.J., Li, K., Fei-Fei, L.: Imagenet: A large-scale hierarchical image database. In: *2009 IEEE conference on computer vision and pattern recognition*. pp. 248–255. Ieee (2009)
13. Devlin, J., Chang, M.W., Lee, K., Toutanova, K.: Bert: Pre-training of deep bidirectional transformers for language understanding. *arXiv preprint arXiv:1810.04805* (2018)
14. Dosovitskiy, A., Beyer, L., Kolesnikov, A., Weissenborn, D., Zhai, X., Unterthiner, T., Dehghani, M., Minderer, M., Heigold, G., Gelly, S., et al.: An image is worth 16x16 words: Transformers for image recognition at scale. *arXiv preprint arXiv:2010.11929* (2020)
15. Esteves, C., Allen-Blanchette, C., Makadia, A., Daniilidis, K.: Learning so (3) equivariant representations with spherical cnns. In: *Proceedings of the European Conference on Computer Vision (ECCV)*. pp. 52–68 (2018)

16. Geiger, A., Lenz, P., Urtasun, R.: Are we ready for Autonomous Driving? The KITTI Vision Benchmark Suite. In: Proc. of the IEEE Conf. on Computer Vision and Pattern Recognition (CVPR). pp. 3354–3361 (2012)
17. Goyal, N., Sachdeva, N., Goel, A., Kalra, J.S., Kumaraguru, P.: Kcnet: Kernel-based canonicalization network for entities in recruitment domain. In: International Conference on Artificial Neural Networks. pp. 157–169. Springer (2021)
18. Graham, B., Engelcke, M., van der Maaten, L.: 3d semantic segmentation with submanifold sparse convolutional networks. CVPR (2018)
19. Gu, X., Wang, Y., Wu, C., Lee, Y.J., Wang, P.: Hplflownet: Hierarchical permutohedral lattice flownet for scene flow estimation on large-scale point clouds. In: Proceedings of the IEEE/CVF Conference on Computer Vision and Pattern Recognition. pp. 3254–3263 (2019)
20. He, K., Zhang, X., Ren, S., Sun, J.: Deep residual learning for image recognition. In: Proceedings of the IEEE conference on computer vision and pattern recognition. pp. 770–778 (2016)
21. Howard, A.G., Zhu, M., Chen, B., Kalenichenko, D., Wang, W., Weyand, T., Andreetto, M., Adam, H.: Mobilenets: Efficient convolutional neural networks for mobile vision applications. arXiv preprint arXiv:1704.04861 (2017)
22. Hu, H., Zhang, Z., Xie, Z., Lin, S.: Local relation networks for image recognition. In: Proceedings of the IEEE/CVF International Conference on Computer Vision. pp. 3464–3473 (2019)
23. Hu, Q., Yang, B., Xie, L., Rosa, S., Guo, Y., Wang, Z., Trigoni, N., Markham, A.: Randla-net: Efficient semantic segmentation of large-scale point clouds. Proceedings of the IEEE Conference on Computer Vision and Pattern Recognition (2020)
24. Hu, Q., Yang, B., Xie, L., Rosa, S., Guo, Y., Wang, Z., Trigoni, N., Markham, A.: Randla-net: Efficient semantic segmentation of large-scale point clouds. In: Proceedings of the IEEE/CVF Conference on Computer Vision and Pattern Recognition. pp. 11108–11117 (2020)
25. Hu, W., Zhao, H., Jiang, L., Jia, J., Wong, T.T.: Bidirectional projection network for cross dimension scene understanding. In: Proceedings of the IEEE/CVF Conference on Computer Vision and Pattern Recognition. pp. 14373–14382 (2021)
26. Hu, Z., Bai, X., Shang, J., Zhang, R., Dong, J., Wang, X., Sun, G., Fu, H., Tai, C.L.: Vmnet: Voxel-mesh network for geodesic-aware 3d semantic segmentation. In: Proceedings of the IEEE/CVF International Conference on Computer Vision. pp. 15488–15498 (2021)
27. Huguet, F., Devernay, F.: A variational method for scene flow estimation from stereo sequences. In: 2007 IEEE 11th International Conference on Computer Vision. pp. 1–7. IEEE (2007)
28. Jampani, V., Kiefel, M., Gehler, P.V.: Learning sparse high dimensional filters: Image filtering, dense crfs and bilateral neural networks. In: Proceedings of the IEEE Conference on Computer Vision and Pattern Recognition. pp. 4452–4461 (2016)
29. Jia, X., De Brabandere, B., Tuytelaars, T., Gool, L.V.: Dynamic filter networks. Advances in neural information processing systems **29**, 667–675 (2016)
30. Kanazaki, A., Matsushita, Y., Nishida, Y.: Rotationnet: Joint object categorization and pose estimation using multiviews from unsupervised viewpoints. In: Proceedings of the IEEE Conference on Computer Vision and Pattern Recognition. pp. 5010–5019 (2018)
31. Kochanov, D., Nejadasl, F.K., Booij, O.: Kprnet: Improving projection-based lidar semantic segmentation. arXiv preprint arXiv:2007.12668 (2020)

32. Kundu, A., Yin, X., Fathi, A., Ross, D., Brewington, B., Funkhouser, T., Pantofaru, C.: Virtual multi-view fusion for 3d semantic segmentation. In: European Conference on Computer Vision. pp. 518–535. Springer (2020)
33. Lai, X., Liu, J., Jiang, L., Wang, L., Zhao, H., Liu, S., Qi, X., Jia, J.: Stratified transformer for 3d point cloud segmentation. In: Proceedings of the IEEE/CVF Conference on Computer Vision and Pattern Recognition. pp. 8500–8509 (2022)
34. Lang, A.H., Vora, S., Caesar, H., Zhou, L., Yang, J., Beijbom, O.: Pointpillars: Fast encoders for object detection from point clouds. In: Proceedings of the IEEE/CVF Conference on Computer Vision and Pattern Recognition. pp. 12697–12705 (2019)
35. Lee, J., Lee, Y., Kim, J., Kosior, A., Choi, S., Teh, Y.W.: Set transformer: A framework for attention-based permutation-invariant neural networks. In: International Conference on Machine Learning. pp. 3744–3753. PMLR (2019)
36. Li, B., Zhang, T., Xia, T.: Vehicle detection from 3d lidar using fully convolutional network. arXiv preprint arXiv:1608.07916 (2016)
37. Li, G., Muller, M., Thabet, A., Ghanem, B.: Deepgcns: Can gcns go as deep as cnns? In: Proceedings of the IEEE/CVF international conference on computer vision. pp. 9267–9276 (2019)
38. Li, R., Lin, G., He, T., Liu, F., Shen, C.: Hcrf-flow: Scene flow from point clouds with continuous high-order crfs and position-aware flow embedding. In: Proceedings of the IEEE/CVF Conference on Computer Vision and Pattern Recognition. pp. 364–373 (2021)
39. Li, X., Li, F., Fern, X., Raich, R.: Filter shaping for convolutional neural networks. In: Proceedings of the International Conference on Learning Representations (ICLR) (2016)
40. Li, X., Wu, W., Fern, X.Z., Fuxin, L.: The devils in the point clouds: Studying the robustness of point cloud convolutions. arXiv preprint arXiv:2101.07832 (2021)
41. Li, Y., Bu, R., Sun, M., Wu, W., Di, X., Chen, B.: Pointcnn: Convolution on x-transformed points. *Advances in neural information processing systems* **31** (2018)
42. Liu, X., Qi, C.R., Guibas, L.J.: Flownet3d: Learning scene flow in 3d point clouds. In: Proceedings of the IEEE/CVF Conference on Computer Vision and Pattern Recognition. pp. 529–537 (2019)
43. Liu, X., Han, Z., Liu, Y.S., Zwicker, M.: Point2sequence: Learning the shape representation of 3d point clouds with an attention-based sequence to sequence network. In: Proceedings of the AAAI Conference on Artificial Intelligence. vol. 33, pp. 8778–8785 (2019)
44. Ma, N., Zhang, X., Huang, J., Sun, J.: Weightnet: Revisiting the design space of weight networks. In: Computer Vision–ECCV 2020: 16th European Conference, Glasgow, UK, August 23–28, 2020, Proceedings, Part XV 16. pp. 776–792. Springer (2020)
45. Mao, J., Wang, X., Li, H.: Interpolated convolutional networks for 3d point cloud understanding. In: Proceedings of the IEEE/CVF International Conference on Computer Vision. pp. 1578–1587 (2019)
46. Maturana, D., Scherer, S.: Voxnet: A 3d convolutional neural network for real-time object recognition. In: 2015 IEEE/RSJ International Conference on Intelligent Robots and Systems (IROS). pp. 922–928. IEEE (2015)
47. Mayer, N., Ilg, E., Häusser, P., Fischer, P., Cremers, D., Dosovitskiy, A., Brox, T.: A large dataset to train convolutional networks for disparity, optical flow, and scene flow estimation. In: IEEE International Conference on Computer Vision and Pattern Recognition (CVPR) (2016), <http://lmb.informatik.uni-freiburg.de/Publications/2016/MIFDB16>, arXiv:1512.02134

48. Mayer, N., Ilg, E., Hausser, P., Fischer, P., Cremers, D., Dosovitskiy, A., Brox, T.: A large dataset to train convolutional networks for disparity, optical flow, and scene flow estimation. In: Proceedings of the IEEE conference on computer vision and pattern recognition. pp. 4040–4048 (2016)
49. Melekhov, I., Tiulpin, A., Sattler, T., Pollefeys, M., Rahtu, E., Kannala, J.: Dgc-net: Dense geometric correspondence network. In: 2019 IEEE Winter Conference on Applications of Computer Vision (WACV). pp. 1034–1042. IEEE (2019)
50. Menze, M., Geiger, A.: Object scene flow for autonomous vehicles. In: Proceedings of the IEEE Conference on Computer Vision and Pattern Recognition. pp. 3061–3070 (2015)
51. Menze, M., Heipke, C., Geiger, A.: Joint 3d estimation of vehicles and scene flow. ISPRS annals of the photogrammetry, remote sensing and spatial information sciences **2**, 427 (2015)
52. Menze, M., Heipke, C., Geiger, A.: Object scene flow. ISPRS Journal of Photogrammetry and Remote Sensing **140**, 60–76 (2018)
53. Nekrasov, A., Schult, J., Litany, O., Leibe, B., Engelmann, F.: Mix3d: Out-of-context data augmentation for 3d scenes. In: 2021 International Conference on 3D Vision (3DV). pp. 116–125. IEEE (2021)
54. Park, C., Jeong, Y., Cho, M., Park, J.: Fast point transformer. arXiv preprint arXiv:2112.04702 (2021)
55. Paszke, A., Gross, S., Massa, F., Lerer, A., Bradbury, J., Chanan, G., Killeen, T., Lin, Z., Gimelshein, N., Antiga, L., et al.: Pytorch: An imperative style, high-performance deep learning library. Advances in neural information processing systems **32** (2019)
56. Puy, G., Boulch, A., Marlet, R.: Flot: Scene flow on point clouds guided by optimal transport. In: Computer Vision—ECCV 2020: 16th European Conference, Glasgow, UK, August 23–28, 2020, Proceedings, Part XXVIII 16. pp. 527–544. Springer (2020)
57. Qi, C.R., Su, H., Mo, K., Guibas, L.J.: Pointnet: Deep learning on point sets for 3d classification and segmentation. In: Proceedings of the IEEE conference on computer vision and pattern recognition. pp. 652–660 (2017)
58. Qi, C.R., Yi, L., Su, H., Guibas, L.J.: Pointnet++: Deep hierarchical feature learning on point sets in a metric space. arXiv preprint arXiv:1706.02413 (2017)
59. Ramachandran, P., Parmar, N., Vaswani, A., Bello, I., Levskaya, A., Shlens, J.: Stand-alone self-attention in vision models. Advances in Neural Information Processing Systems **32** (2019)
60. Riegler, G., Osman Ulusoy, A., Geiger, A.: Octnet: Learning deep 3d representations at high resolutions. In: Proceedings of the IEEE conference on computer vision and pattern recognition. pp. 3577–3586 (2017)
61. Shaw, P., Uszkoreit, J., Vaswani, A.: Self-attention with relative position representations. arXiv preprint arXiv:1803.02155 (2018)
62. Simonovsky, M., Komodakis, N.: Dynamic edge-conditioned filters in convolutional neural networks on graphs. In: Proceedings of the IEEE conference on computer vision and pattern recognition. pp. 3693–3702 (2017)
63. Song, S., Yu, F., Zeng, A., Chang, A.X., Savva, M., Funkhouser, T.: Semantic scene completion from a single depth image. In: Proceedings of the IEEE conference on computer vision and pattern recognition. pp. 1746–1754 (2017)
64. Su, H., Jampani, V., Sun, D., Gallo, O., Learned-Miller, E., Kautz, J.: Pixel-adaptive convolutional neural networks. In: Proceedings of the IEEE/CVF Conference on Computer Vision and Pattern Recognition. pp. 11166–11175 (2019)

65. Su, H., Jampani, V., Sun, D., Maji, S., Kalogerakis, E., Yang, M.H., Kautz, J.: Splatnet: Sparse lattice networks for point cloud processing. In: Proceedings of the IEEE conference on computer vision and pattern recognition. pp. 2530–2539 (2018)
66. Su, H., Maji, S., Kalogerakis, E., Learned-Miller, E.: Multi-view convolutional neural networks for 3d shape recognition. In: Proceedings of the IEEE international conference on computer vision. pp. 945–953 (2015)
67. Tabernik, D., Kristan, M., Leonardis, A.: Spatially-adaptive filter units for compact and efficient deep neural networks. *International Journal of Computer Vision* **128**(8), 2049–2067 (2020)
68. Tang, H., Liu, Z., Zhao, S., Lin, Y., Lin, J., Wang, H., Han, S.: Searching efficient 3d architectures with sparse point-voxel convolution. In: European conference on computer vision. pp. 685–702. Springer (2020)
69. Thomas, H., Qi, C.R., Deschaud, J.E., Marcotegui, B., Goulette, F., Guibas, L.J.: Kpconv: Flexible and deformable convolution for point clouds. In: Proceedings of the IEEE/CVF International Conference on Computer Vision. pp. 6411–6420 (2019)
70. Tian, Z., Shen, C., Chen, H.: Conditional convolutions for instance segmentation. In: Computer Vision–ECCV 2020: 16th European Conference, Glasgow, UK, August 23–28, 2020, Proceedings, Part I 16. pp. 282–298. Springer (2020)
71. Vaswani, A., Shazeer, N., Parmar, N., Uszkoreit, J., Jones, L., Gomez, A.N., Kaiser, L., Polosukhin, I.: Attention is all you need. In: Advances in neural information processing systems. pp. 5998–6008 (2017)
72. Vogel, C., Schindler, K., Roth, S.: 3d scene flow estimation with a piecewise rigid scene model. *International Journal of Computer Vision* **115**(1), 1–28 (2015)
73. Wang, C., Samari, B., Siddiqi, K.: Local spectral graph convolution for point set feature learning. In: Proceedings of the European conference on computer vision (ECCV). pp. 52–66 (2018)
74. Wang, J., Chen, K., Xu, R., Liu, Z., Loy, C.C., Lin, D.: Carafe: Content-aware reassembly of features. In: Proceedings of the IEEE/CVF International Conference on Computer Vision. pp. 3007–3016 (2019)
75. Wang, S., Suo, S., Ma, W.C., Pokrovsky, A., Urtasun, R.: Deep parametric continuous convolutional neural networks. In: Proceedings of the IEEE Conference on Computer Vision and Pattern Recognition. pp. 2589–2597 (2018)
76. Wang, X., Girshick, R., Gupta, A., He, K.: Non-local neural networks. In: Proceedings of the IEEE conference on computer vision and pattern recognition. pp. 7794–7803 (2018)
77. Wang, X., Zhang, R., Kong, T., Li, L., Shen, C.: Solov2: Dynamic, faster and stronger. arXiv e-prints pp. arXiv–2003 (2020)
78. Wei, Y., Wang, Z., Rao, Y., Lu, J., Zhou, J.: Pv-raft: Point-voxel correlation fields for scene flow estimation of point clouds. In: Proceedings of the IEEE/CVF Conference on Computer Vision and Pattern Recognition. pp. 6954–6963 (2021)
79. Wu, F., Fan, A., Baevski, A., Dauphin, Y.N., Auli, M.: Pay less attention with lightweight and dynamic convolutions. arXiv preprint arXiv:1901.10430 (2019)
80. Wu, W., Qi, Z., Fuxin, L.: Pointconv: Deep convolutional networks on 3d point clouds. In: Proceedings of the IEEE/CVF Conference on Computer Vision and Pattern Recognition. pp. 9621–9630 (2019)
81. Wu, W., Wang, Z.Y., Li, Z., Liu, W., Fuxin, L.: Pointpwc-net: Cost volume on point clouds for (self-) supervised scene flow estimation. In: European Conference on Computer Vision. pp. 88–107. Springer (2020)

82. Xie, S., Liu, S., Chen, Z., Tu, Z.: Attentional shapecontextnet for point cloud recognition. In: Proceedings of the IEEE Conference on Computer Vision and Pattern Recognition. pp. 4606–4615 (2018)
83. Xu, Y., Fan, T., Xu, M., Zeng, L., Qiao, Y.: Spidercnn: Deep learning on point sets with parameterized convolutional filters. In: Proceedings of the European Conference on Computer Vision (ECCV). pp. 87–102 (2018)
84. Yan, X., Zheng, C., Li, Z., Wang, S., Cui, S.: Pointasnl: Robust point clouds processing using nonlocal neural networks with adaptive sampling. In: Proceedings of the IEEE/CVF Conference on Computer Vision and Pattern Recognition. pp. 5589–5598 (2020)
85. Yang, B., Bender, G., Le, Q.V., Ngiam, J.: Condconv: Conditionally parameterized convolutions for efficient inference. arXiv preprint arXiv:1904.04971 (2019)
86. Yang, J., Zhang, Q., Ni, B., Li, L., Liu, J., Zhou, M., Tian, Q.: Modeling point clouds with self-attention and gumbel subset sampling. In: Proceedings of the IEEE/CVF Conference on Computer Vision and Pattern Recognition. pp. 3323–3332 (2019)
87. Yang, Z., Dai, Z., Yang, Y., Carbonell, J., Salakhutdinov, R.R., Le, Q.V.: Xlnet: Generalized autoregressive pretraining for language understanding. *Advances in neural information processing systems* **32** (2019)
88. Zamora Esquivel, J., Cruz Vargas, A., Lopez Meyer, P., Tickoo, O.: Adaptive convolutional kernels. In: Proceedings of the IEEE/CVF International Conference on Computer Vision Workshops. pp. 0–0 (2019)
89. Zhang, F., Fang, J., Wah, B., Torr, P.: Deep fusionnet for point cloud semantic segmentation. In: European Conference on Computer Vision. pp. 644–663. Springer (2020)
90. Zhang, Y., Zhang, J., Wang, Q., Zhong, Z.: Dynet: Dynamic convolution for accelerating convolutional neural networks. arXiv preprint arXiv:2004.10694 (2020)
91. Zhang, Z., Hua, B.S., Rosen, D.W., Yeung, S.K.: Rotation invariant convolutions for 3d point clouds deep learning. In: 2019 International conference on 3d vision (3DV). pp. 204–213. IEEE (2019)
92. Zhao, H., Jia, J., Koltun, V.: Exploring self-attention for image recognition. In: Proceedings of the IEEE/CVF Conference on Computer Vision and Pattern Recognition. pp. 10076–10085 (2020)
93. Zhao, H., Jiang, L., Jia, J., Torr, P.H., Koltun, V.: Point transformer. In: Proceedings of the IEEE/CVF International Conference on Computer Vision. pp. 16259–16268 (2021)
94. Zhou, J., Jampani, V., Pi, Z., Liu, Q., Yang, M.H.: Decoupled dynamic filter networks. In: Proceedings of the IEEE/CVF Conference on Computer Vision and Pattern Recognition. pp. 6647–6656 (2021)
95. Zhu, X., Zhou, H., Wang, T., Hong, F., Ma, Y., Li, W., Li, H., Lin, D.: Cylindrical and asymmetrical 3d convolution networks for lidar segmentation. In: Proceedings of the IEEE/CVF conference on computer vision and pattern recognition. pp. 9939–9948 (2021)

Appendix

A Network Structure

A.1 Network structure for semantic segmentation

As in Fig. 10, we use a U-Net structure for semantic segmentation tasks. The U-Net contains 5 resolution levels. For each resolution level, we use grid subsampling to downsample the input point clouds, then followed by several pointconvformer residual blocks. For deconvolution, we just use PointConv as described in the main paper.

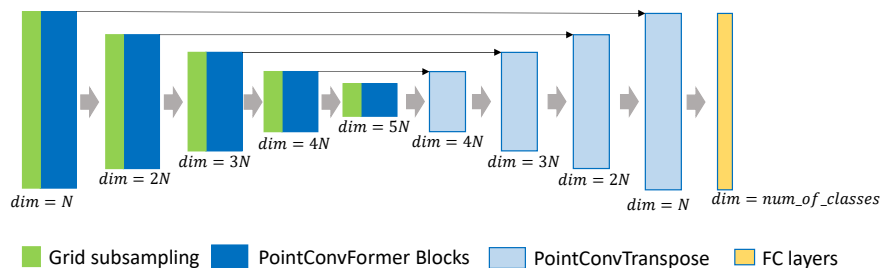


Fig. 10: **The network structure of semantic segmentation.** We use a U-Net structure for semantic segmentation tasks. The U-Net contains 5 resolution levels. For each resolution level, we use grid subsampling to downsample the input point clouds, then followed by several pointconvformer residual blocks. For deconvolution, we just use PointConv as described in the main paper. We set $N = 64$ for ScanNet [10] Dataset and $N = 48$ for SemanticKitti [2] Dataset. (Best viewed in color.)

A.2 Network structure for scene flow estimation

Fig. 11 illustrates the network structure we used for scene flow estimation. Following the network structure of PointPWC-Net [81], which is a coarse-to-fine network design, the PCFPWC-Net also contains 5 modules, including the feature pyramid network, cost volume layers, upsampling layers, warping layers, and the scene flow predictors. We replace the PointConv in the Feature pyramid layers with the PointConvFormer and keep the rest of the structure the same as the original version of PointPWC-Net for fair comparison.

B Evaluation Metrics for Scene flow estimation

Evaluation Metrics. For comparison, we use the same metrics as [81]. Let SF_{θ} denote the predicted scene flow, and SF_{GT} be the ground truth scene flow. The evaluate metrics are computed as follows:

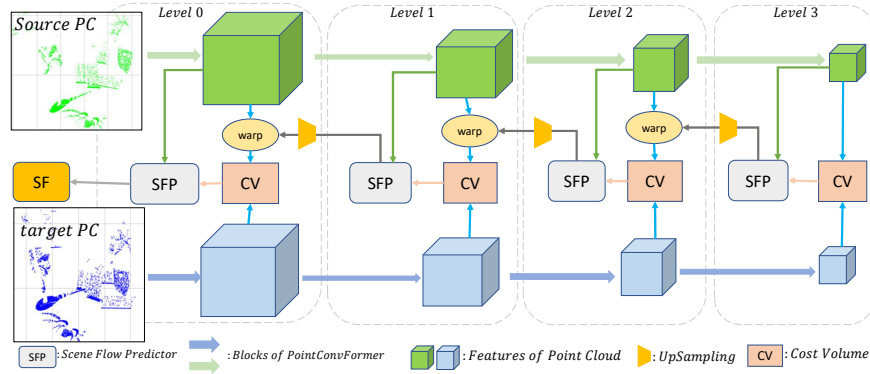


Fig. 11: **The network structure of PointPWC-Net with PointConvFormer.** The feature pyramid is built with blocks of PointConvFormers. As a result, there are 4 resolution levels in the PointPWC-Net. At each level, the features of the source point cloud are warped according to the upsampled coarse flow. Then, the cost volume are computed using the warped source features and target features. Finally, the scene flow predictor predicts finer flow at the current level using a PointConv with features from the first point cloud, the cost volume, and the upsampled flow. (Best viewed in color.)

- $EPE3D(m)$: $\|SF_{\Theta} - SF_{GT}\|_2$ averaged over each point in meters.
- $Acc3DS$: the percentage of points with $EPE3D < 0.05m$ or relative error $< 5\%$.
- $Acc3DR$: the percentage of points with $EPE3D < 0.1m$ or relative error $< 10\%$.
- $Outliers3D$: the percentage of points with $EPE3D > 0.3m$ or relative error $> 10\%$.
- $EPE2D(px)$: 2D end point error obtained by projecting point clouds back to the image plane.
- $Acc2D$: the percentage of points whose $EPE2D < 3px$ or relative error $< 5\%$.

C Ablation Study

Following the same setup as in the main paper, we conduct ablation studies by disabling each component of the PointConvFormer in turn. Table. 10 reports the experiment results. Without the convolution weights or the reweighted score, the performance drops more than 3% comparing the full PointConvFormer, indicating the effectiveness of our design.

D More Visualizations

D.1 More Visualization

In this section, we report more visualization of the prediction of our PointConvFormer. Fig. 12 is the visualization of the comparison between PointConv [80],

Table 10: **Ablation Study.** We disable each component of the PointConvFormer in turn.

Rewighted score	Conv	mIoU(%)
✓	✓	65.78
	✓	65.20
✓	✓	69.16

Point Transformer [93] and PointConvFormer on the ScanNet dataset [10]. Fig. 13 illustrates the prediction of PointConvFormer on the SemanticKitti dataset [2]. Fig. 14 and Fig. 15 are the comparison between the prediction of PointPWC [81] and PCFPWC-Net on the FlyingThings3D [47] and the KITTI Scene Flow 2015 dataset [51]. Please also refer to the video for better visualization.

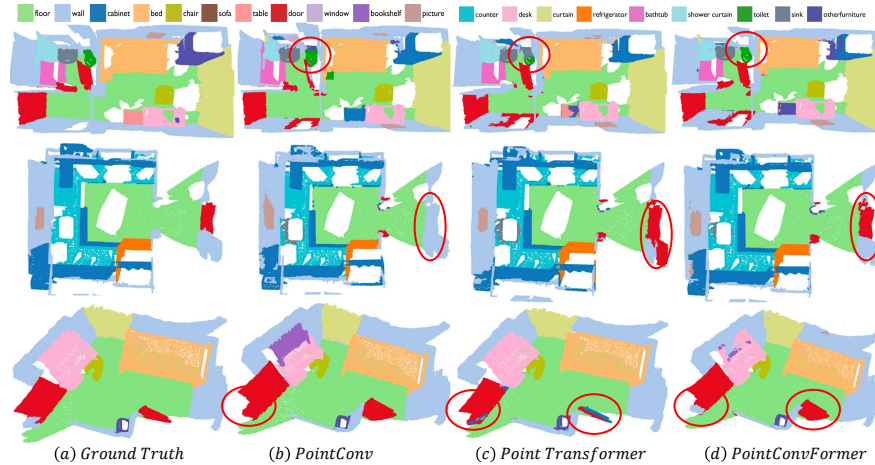


Fig. 12: **ScanNet result visualization.** We visualize the ScanNet prediction results from our PointConvFormer, PointConv [80] and Point Transformer [93]. The red ellipses indicates the improvements of our PointConvFormer over other approaches. Points with ignore labels are filtered for a better visualization. (Best viewed in color)

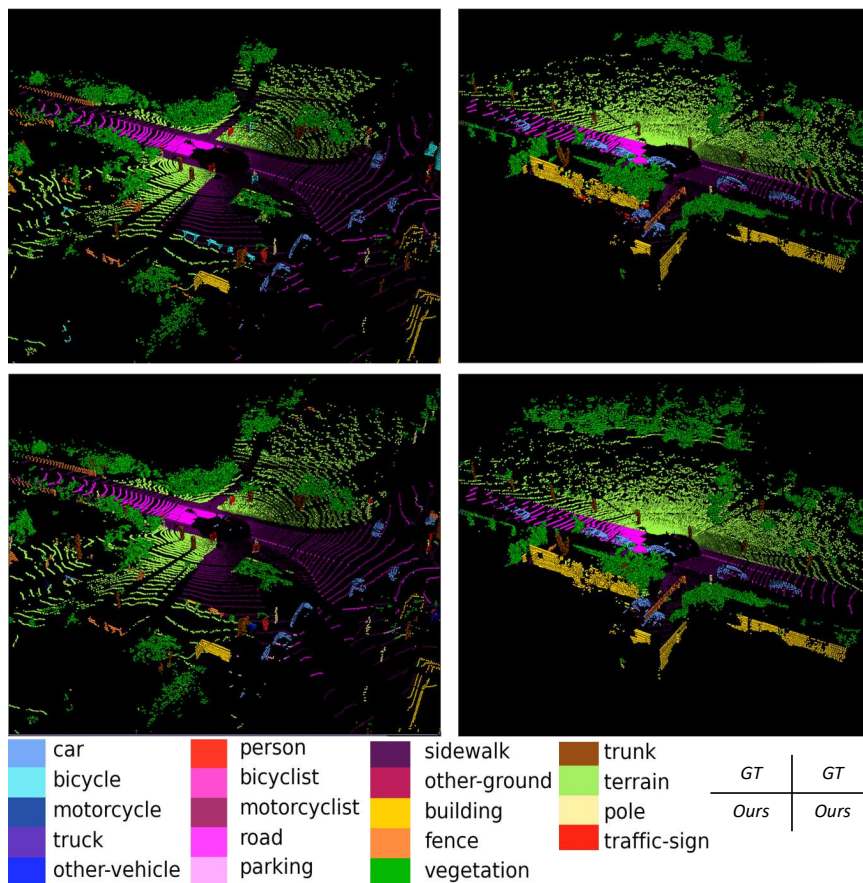


Fig. 13: **SemanticKitti result visualization.** We visualize the SemanticKitti prediction results from our PointConvFormer. Each column is a scan from SemanticKitti validation set. The first row is the input, the second row is the ground truth, the third row is our prediction. (Best viewed in color.)

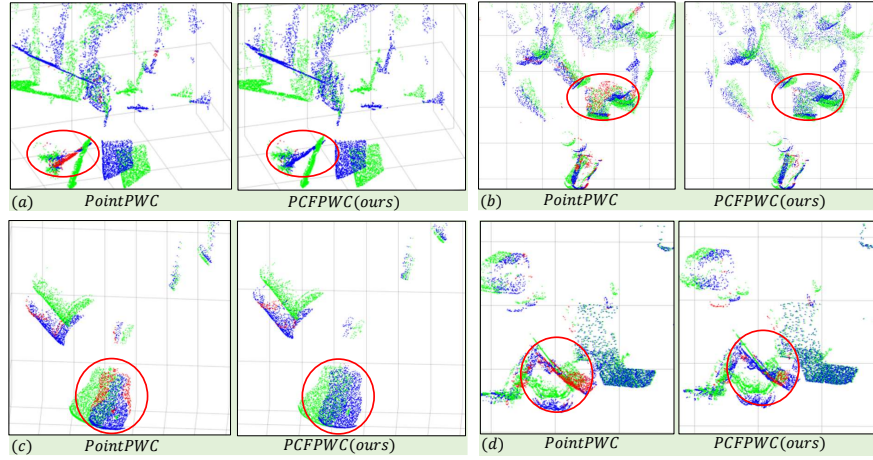


Fig. 14: **Qualitative comparison between PointPWC-Net and PCFPWC-Net (FlyingThings3D [48]).** (a) is the visualization of the FlyingThings3D dataset. (b) is the visualization of the KITTI dataset. Green points are the source point cloud. Blue points are the points warped by the correctly predicted scene flow. The predicted scene flow belonging to Acc3DR is regarded as a correct prediction. For the points with incorrect predictions, we use the ground truth scene flow to warp them and the warped results are shown as red points. (Best viewed in color.)

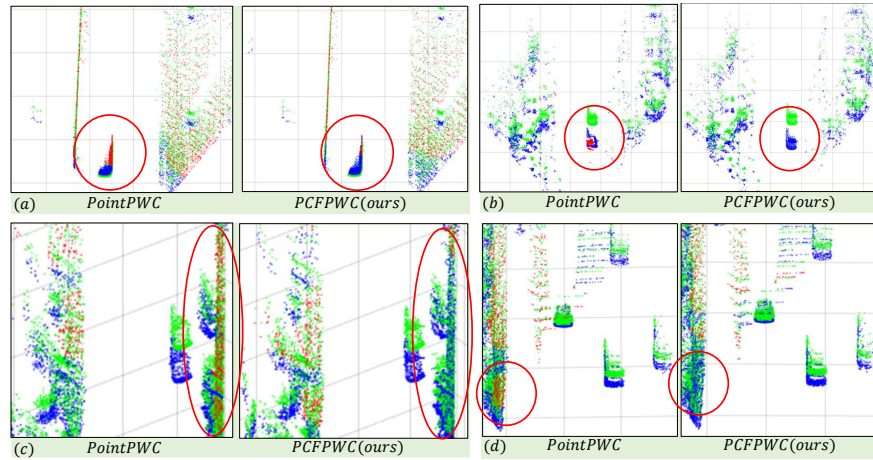


Fig. 15: **Qualitative comparison between PointPWC-Net and PCFPWC-Net (KITTI [51]).** Green points are the source point cloud. Blue points are the points warped by the correctly predicted scene flow. The predicted scene flow belonging to Acc3DR is regarded as a correct prediction. For the points with incorrect predictions, we use the ground truth scene flow to warp them and the warped results are shown as red points. (d) is a failure case, where the points on the wall or ground/road are hard to find accurate correspondences for both PointPWC and PCFPWC. (Best viewed in color.)